JOURNAL OF MATERIALS SCIENCE **40** (2005) 3445–3452

Infrared brazing Inconel 601 and 422 stainless steel using the 70Au-22Ni-8Pd braze alloy

Y. K. YU, D. W. LIAW
Department of Materials Science and Engineering, National Dong Hwa University, Hualien 974, Taiwan, Republic of China

R. K. SHIUE*
Department of Materials Science and Engineering, National Taiwan University, Taipei 106, Taiwan, Republic of China
E-mail: rkshiue@ntu.edu.tw

Infrared brazing Inconel 601 and 422 stainless steel using the 70Au-22Ni-8Pd braze alloy is performed in the experiment. The brazed joint is primarily comprised of Au-rich and Ni-rich phases, and there is no interfacial intermetallic compound observed in the joint. The (Ni,Fe)-rich phase is observed at the interface between 422SS and the braze alloy, and the Ni-rich phase is found at the interface between the braze alloy and IN601. With increasing the brazing temperature and/or time, the microstructures of the brazed joint is coarsened. For the infrared brazed joint at 1050°C for 180 s shows the highest average shear strength of 362 MPa. In contrast, the shear strength of the infrared brazed joint is higher than that of the furnace brazed specimen due to coarsening of the microstructure in the furnace brazed joint.

1. Introduction

Inconel 601 (IN601) has the nominal composition of 23% Cr, 14.1% Fe, 0.5% Mn, 0.2% Si, 1.4% Al and Ni balance in weight percent [1]. It is a general-purpose engineering alloy for applications requiring heat and corrosion resistance such as radiant furnace tubes, furnace muffles and retorts. The high chromium content of this nickel-base alloy provides good corrosion resistance to many environments as well as high-temperature oxidation resistance. Additionally, minor aluminum content also enhances its oxidation resistance [1, 2]. AISI 422 stainless steel (422SS) is a type of high strength martensitic stainless steel with the nominal composition of 12% Cr, 0.22% C, 1.0% Mo, 0.25% V, 1.0% W and Fe balance in weight percent [1]. It can be used as steam turbine blades and fasteners at service temperatures up to 650°C. Accordingly, both IN601 and 422SS are structural alloys used in medium and/or high temperatures.

Brazing is widely accepted as one of the most popular ways in joining dissimilar alloys [3–6]. Gold-based filler metals have been used to braze iron, nickel and cobalt-based alloys where resistance to oxidation or corrosion is required. They are commonly used on thin sections due to their low rate of interaction with many base metals [6]. 70Au-22Ni-8Pd braze alloy is a type of gold-based braze alloy, and it is selected as the brazing filler metal in the experiment.

Infrared brazing is a novel brazing process due to its very rapid thermal cycle, and many successful joints have been made in previous studies [7–12]. This research is focused in infrared brazing IN601 and 422SS using the 70Au-22Ni-8Pd braze alloy. Both traditional furnace brazing and infrared brazing are employed in the experiment for the purpose of comparison. Additionally, microstructural evolution and shear strength of the brazed joint with various brazing conditions have also been widely evaluated in this work.

2. Experimental procedures

Base metals used in the experiment were IN601 and 422SS plates with dimension of 10 mm × 10 mm × 3 mm. The substrate was polished with SiC papers up to 1200 grit, and subsequently cleaned using an ultrasonic bath with acetone as the fluid before brazing. Palniro-7 foil with 50 μm thick and 25 mm wide was purchased from Wesgo Metals Inc., and its nominal composition in weight percent is 22% Ni, 8% Pd and Au balance. According to the American Welding Society (AWS), the chemical composition of the Palniro-7 braze alloy is in accordance with the BAu-6 braze alloy [3]. Its solidus and liquidus temperatures are 1010 and 1045°C, respectively.

Both furnace and infrared brazing were performed in the experiment with a vacuum of 5×10^{-5} mbar at various brazing conditions. The heating rate of conventional vacuum furnace was 30°C/min, and the heating rate of infrared furnace was kept at 600°C/min throughout the experiment. All brazed specimens were

*Author to whom all correspondence should be addressed.

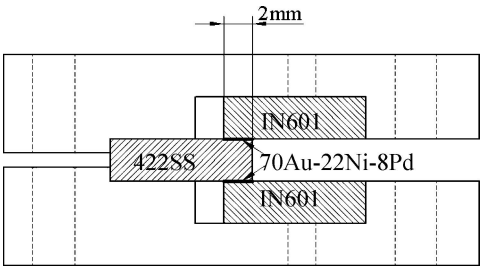

Figure 1 The schematic diagram of the shear test specimen.

preheated at 600°C for 600 s before the brazing temperature was reached. Table I summarizes all brazing conditions used in the test.

The cross section of the brazed specimen was examined using a Hitachi 3500H scanning electron microscope (SEM) with the accelerating voltage of 20 kV. Chemical analyses were performed using energy-dispersive X-ray spectrometer (EDS) with an operation voltage of 20 kV and minimum spot size of 1 μm. The shear test was performed in order to evaluate the bonding strength of the brazed specimen [7, 8, 11]. Fig. 1 shows the schematic diagram of the shear test specimen used in this experiment. The middle shaded area is the 422SS substrate, and two IN601 substrates are located at the outer shaded areas next to the 422SS. The outer part of the layout is the specimen holder used in brazing. Additionally, two bold black lines with 2.0 mm width at the middle of the graph indicate the location of 70Au-22Ni-8Pd braze alloy. Shear tests were made using a Shimadzu AG-10 universal testing machine with a constant crosshead speed of 0.5 mm/min [7, 8, 11]. The cross section of the above fractured specimen was mounted in an epoxy, and examined by an SEM in order to perform failure analysis of the fractured joint.

TABLE I The brazing condition used in the experiment

Types of brazing	Temperature (°C)	Time (s)	Heating rate
Infrared brazing	1050	180, 300	600°C/min
Infrared brazing	1100	180, 300	600°C/min
Furnace brazing	1050	1200	30°C/min

3. Results and discussion

Fig. 2 displays the SEM secondary electron image (SEI), backscattered electron images (BEIs) and chemical analysis results of the furnace brazed 422SS/70Au-22Ni-8Pd/IN601 specimen at 1050°C for 1200 s.

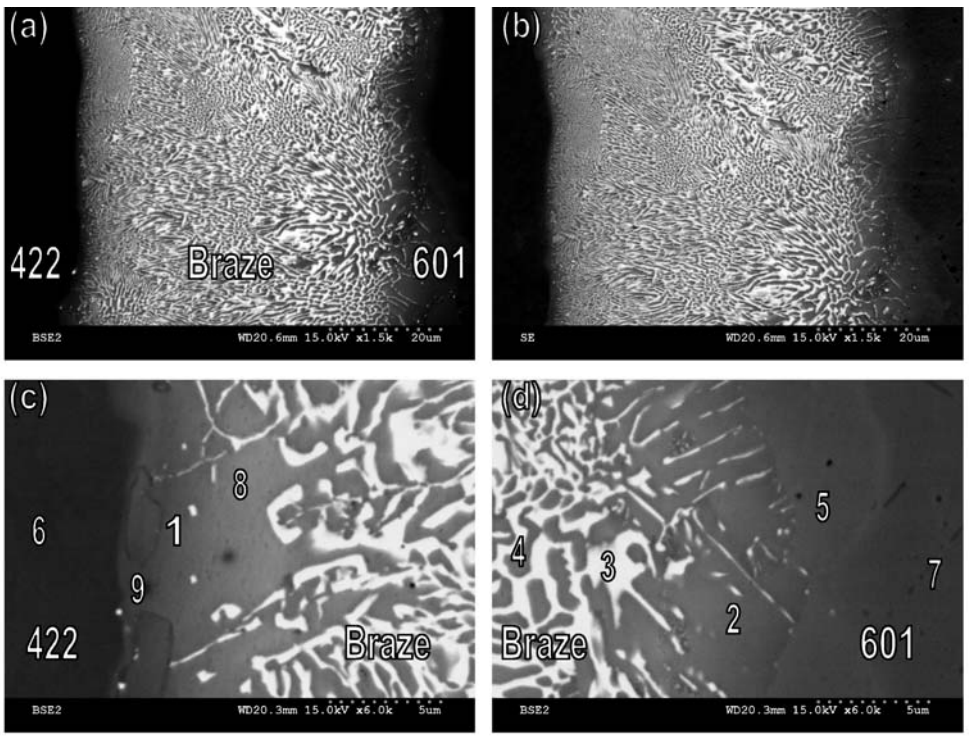

Location (phase)	Au	Pd	Ni	Si	Cr	Mo	V	W	Fe	Mn	Al
1 (Fe,Ni)	6.8	2.6	23.4	2.7	8.8	0.0	0.1	1.4	54.0	0.2	0.1
2 (Ni-rich)	4.0	1.7	61.7	2.2	14.7	0.0	0.1	0.2	14.8	0.0	0.7
3 (Au-rich)	57.2	8.6	12.1	7.5	6.6	0.0	0.2	1.3	5.9	0.3	0.3
4 (Ni-rich)	7.9	1.9	64.1	3.9	6.1	0.0	0.0	0.1	15.1	0.4	0.6
5 (Ni-rich)	1.0	0.2	59.0	0.7	22.2	0.0	0.0	0.6	14.4	0.2	1.8
6 (422SS)	0.4	0.1	0.9	1.6	12.1	0.5	0.2	0.3	83.0	0.9	0.1
7 (IN601)	0.5	0.0	57.1	0.5	23.8	0.0	0.2	0.0	15.2	0.1	2.6
8 (Fe,Ni)	8.3	3.3	30.3	3.3	7.4	0.0	0.3	0.6	46.1	0.4	0.1
9 (Fe,Ni)	2.0	1.6	19.6	2.2	9.2	0.0	0.2	0.3	64.5	0.3	0.3

Figure 2 SEM images and chemical analysis results of the furnace brazed specimen in atomic percent at 1050°C for 1200 s: (a) (c) (d) BEIs and (b) SEI.

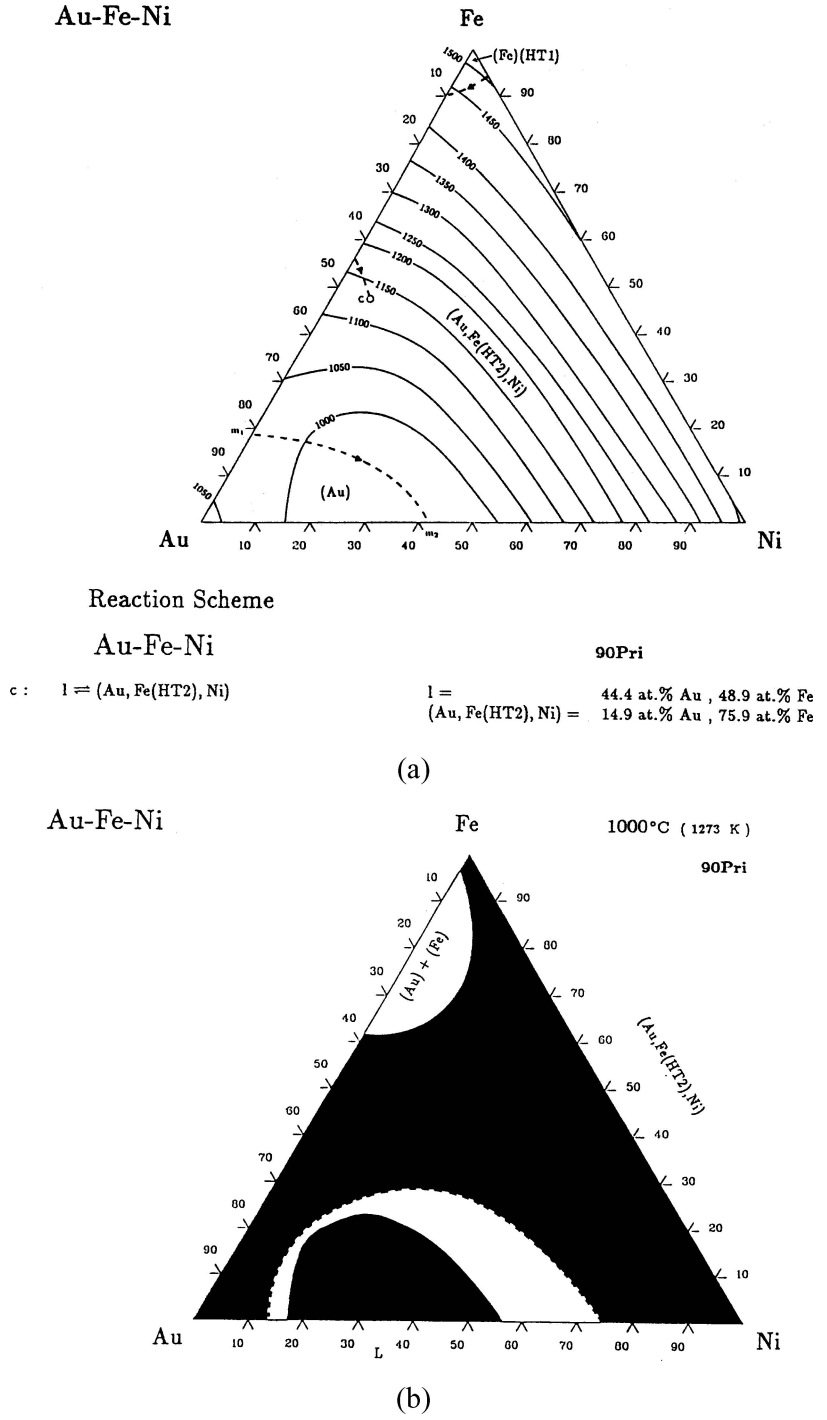

Figure 3 Au-Fe-Ni ternary alloy phase diagrams (a) liquidus projection and (b) isothermal section at 1000°C [13].

According to the EDS analysis results, the furnace brazed joint primarily consists of Au-rich (marked by point 3) and Ni-rich (marked by point 4) phases. The chemical composition of the 70Au-22Ni-8Pd braze alloy in atomic percent is 44.1% Au, 46.5% Ni and 9.4% Pd. Based on the Au-Ni-Pd ternary alloy phase diagram, the molten braze zones prone to be separated into two phases, the Au-rich and Ni-rich phases [13, 14]. Additionally, the Au-rich phase can dissolve Pd and Ni, and the Ni-rich phase dissolves Pd and Au. It is consistent with the experimental observations.

It is important to note that there is no interfacial reaction compound observed in both 422SS/braze and braze/IN601 interfaces. For the interface between 422SS and the braze alloy, the interfacial (Fe,Ni)-rich phase is observed as marked by points 1, 8 and 9 in Fig. 2. In contrast, the Ni-rich phase is observed at the interface between the braze alloy and IN601 as marked by points 2 and 5. Since Au, Fe and Ni are major constituents in the EDS chemical analysis as shown in Fig. 2, the Au-Fe-Ni ternary alloy phase diagram is cited here in order to illustrate the microstructural evolution of the furnace brazed joint.

Fig. 3a shows the liquidus projection of the Au-Fe-Ni ternary alloy phase diagram, and the important reaction scheme is also included in the figure. It is clear that dissolution of either the nickel-based IN601 or the iron-based 422SS substrates into the molten braze significantly increases the melting point of the braze alloy. Accordingly, isothermal solidification of the molten braze

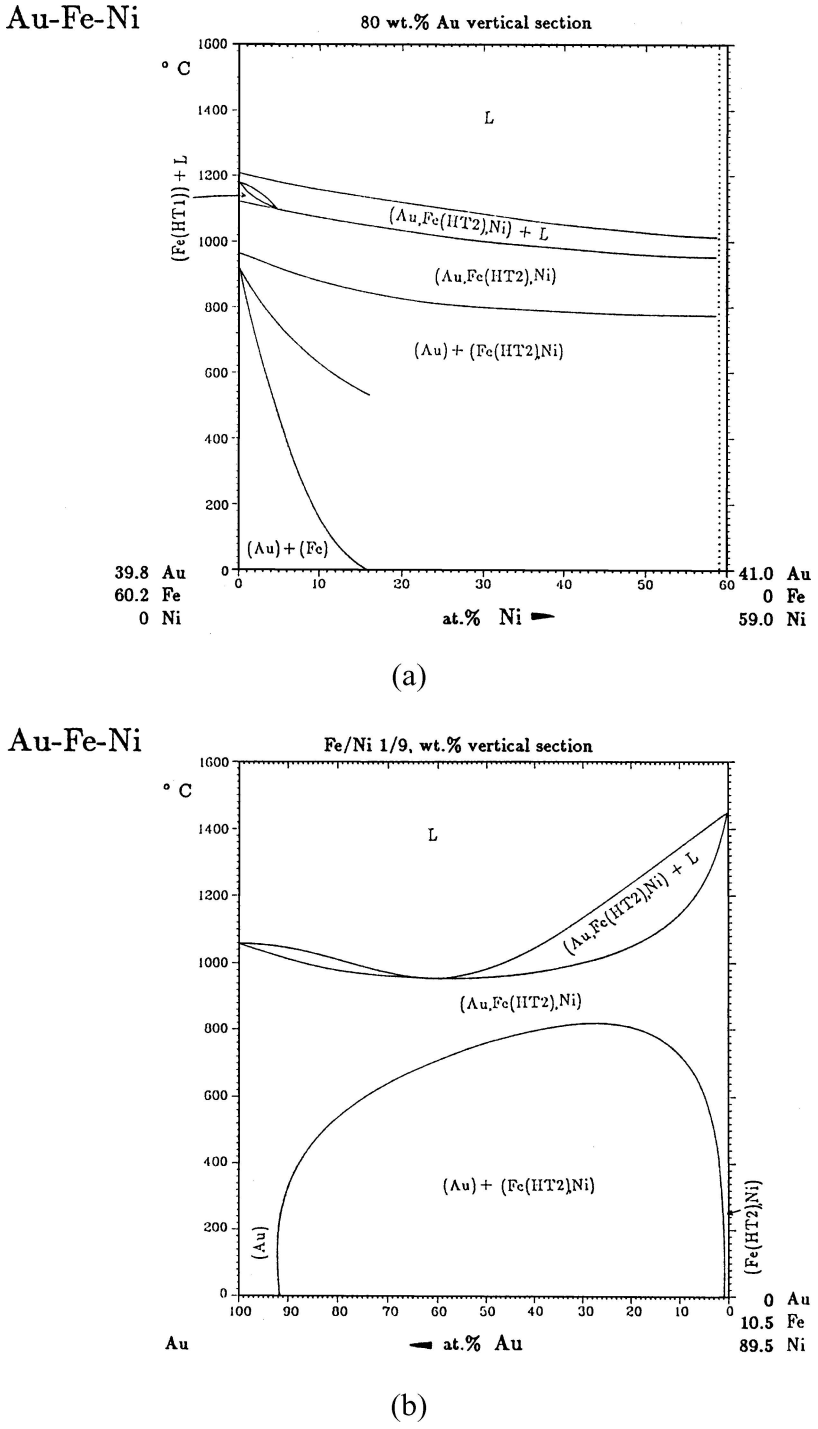

Figure 4 Two vertical sections of the Au-Fe-Ni pseudobinary phase diagrams: (a) 80 wt% Au vertical section and (b) (Fe/Ni) = (1/9) wt% vertical section [13].

can be observed especially at the interface between the braze alloy and substrate because of the molten braze alloyed with high contents of Fe or Ni. Fig. 3b shows the isothermal thermal section of Au-Fe-Ni at 1000°C [13]. Based on this figure, there are two immiscibility gaps, Au-Ni and Au-Fe, at 1000°C. In contrast, the Fe is completely miscible with the Ni at 1000°C. During brazing, the molten braze alloy is initially comprised of mainly Au and Ni, and it tends to be separated into two immiscible liquids, the Au-rich and Ni-rich liquids. Both substrates are simultaneously dissolved into the molten braze, so the iron content of the braze alloy is increased.

Fig. 4 shows two vertical sections of the Au-Fe-Ni pseudobinary phase diagrams [13]. Two important features can be derived from the figure. First, there is no intermetallic compound found in these figures. Second, both Au-rich and (Fe,Ni)-rich phases are observed in the figure. According to the EDS analyses in Fig. 2, the (Fe,Ni)-rich phase is observed at the interface between 422SS and the braze alloy. They are consistent with the experimental results.

Fig. 5 display the SEM BEIs and EDS chemical analysis results of infrared brazed joints at 1050°C for 180 and 300 s, respectively. Accurate cooling rates for the different brazing time periods cannot be precisely

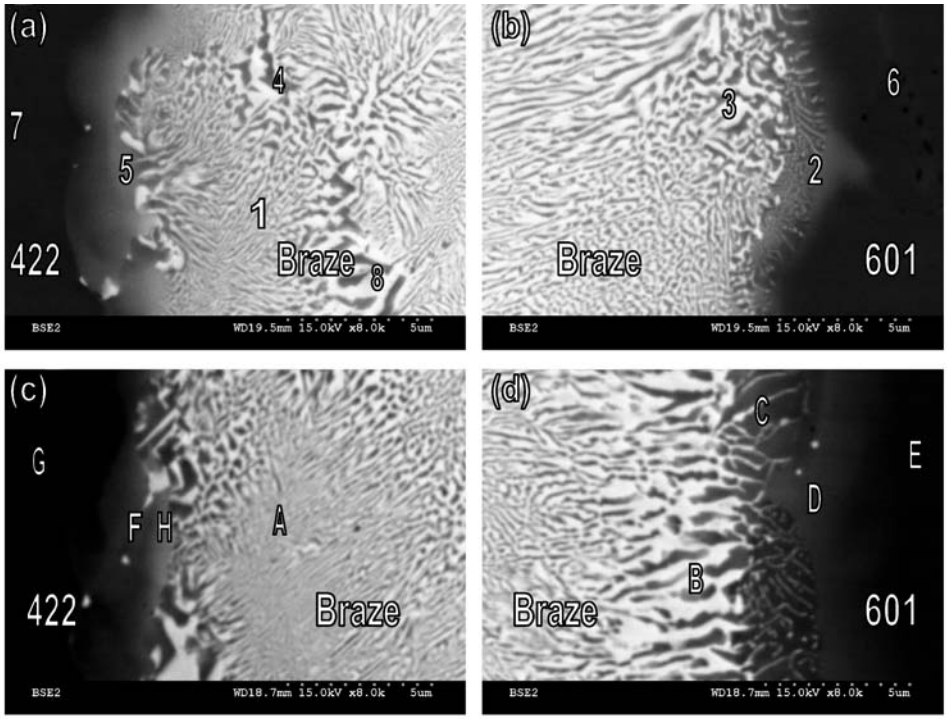

Location (phase)	Au	Pd	Ni	Si	Cr	Mo	V	W	Fe	Mn	Al
1 ((Fe,Ni)+Au)	27.0	7.9	34.4	5.0	3.4	0.0	0.2	0.8	21.4	0.0	0.0
2 (Ni-rich)	5.1	2.1	67.1	1.5	13.1	0.0	0.0	0.3	10.5	0.1	0.2
3 (Au-rich)	42.5	9.5	26.7	6.8	6.4	0.0	0.0	0.4	5.7	0.3	1.6
4 (Ni-rich)	2.4	1.4	61.3	1.6	18.5	0.0	0.0	0.4	12.7	0.3	1.4
5 (Fe,Ni)	6.0	2.7	24.1	2.9	7.4	0.0	0.2	1.3	55.2	0.1	0.1
6 (IN 601)	0.0	0.0	57.4	0.5	23.7	0.0	0.2	0.4	14.6	0.2	2.9
7 (422SS)	0.5	0.1	1.0	1.7	12.7	0.6	0.4	0.2	82.0	0.7	0.0
8 (Au-rich)	44.2	11.8	26.8	6.8	5.1	0.0	0.2	0.4	4.8	0.1	0.0
A ((Fe,Ni)+Au)	34.5	8.2	37.4	5.7	2.2	0.0	0.4	0.0	11.7	0.1	0.0
B (Au-rich)	44.3	11.1	29.4	5.9	5.9	0.0	0.0	0.0	3.5	0.0	0.0
C (Ni-rich)	10.8	4.0	64.8	2.2	8.9	0.0	0.2	0.5	8.4	0.1	0.2
D (Ni-rich)	6.1	2.6	63.0	1.8	14.9	0.0	0.2	0.3	10.4	0.1	0.6
E (IN 601)	0.0	0.0	56.9	0.6	23.8	0.2	0.1	0.5	15.5	0.1	2.3
F (Fe-rich)	1.6	0.8	8.3	2.1	10.5	0.0	0.2	0.3	75.8	0.5	0.0
G (422SS)	0.1	0.1	0.8	1.6	11.8	0.4	0.5	0.6	83.1	0.9	0.1
H (Fe,Ni)	8.5	2.2	24.0	3.0	7.6	0.0	0.0	1.3	53.1	0.1	0.2

Figure 5 The SEM BEIs and EDS chemical analysis results of infrared brazed joints at 1050°C for (a)(b) 180 s and (c)(d) 300 s.

determined in the experiment. However, both specimens are furnace cooled from 1050°C to room temperature. It is reasonable to conclude that cooling rates for the different brazing time periods, 180 and 300 s, are approximately the same. Difference in microstructure between infrared brazed joints for 180 and 300 s brazing time is not significant, except for Inconel side, where some coarsening is visible. Additionally, the microstructure of infrared brazed joints is very similar to that of the furnace brazed specimen except for the infrared brazed joint with a finer microstructure as compared between Figs 2 and 5. Similar to the aforementioned result, the infrared brazed joint is primarily comprised of Au-rich and Ni-rich phases. Additionally, the (Fe,Ni)-rich phase as marked by points 5 and H is observed at the interface between 422SS and the braze alloy. The Ni-rich phase is observed at the interface between the braze alloy and IN601 as marked by points 2, C and D. The thickness of both interfacial (Fe,Ni)-rich and Ni-rich phases are significantly decreased for the infrared brazed specimen due to its rapid brazing cycle. Accordingly, the erosion of base metals is greatly reduced for the infrared brazed specimen.

Fig. 6 shows the SEM BEIs and EDS chemical analysis results of infrared brazed joints at 1100°C for 180 and 300 s, respectively. The infrared brazed specimen is mainly comprised of Au-rich (marked by points 3 and C) and Ni-rich (marked by points 2, 4, B and G) phases. It is important to note that the microstructure of the infrared brazed joint at 1100°C is greatly coarsened as compared with that of the infrared brazed specimen at 1050°C (Fig. 5). Moreover, the growth of both interfacial (Fe,Ni)-rich and Ni-rich phases is greatly enhanced as shown in Fig. 6e. As discussed earlier, the dissolution of base metal into the molten braze and interdiffusion among the braze alloy and two substrates are greatly increased with increasing the brazing temperature. Accordingly, enhanced metallurgical phenomena among the braze alloy and two substrates are widely observed in the experiment.

Table II displays shear strengths of various brazed specimens with different brazing conditions. Because

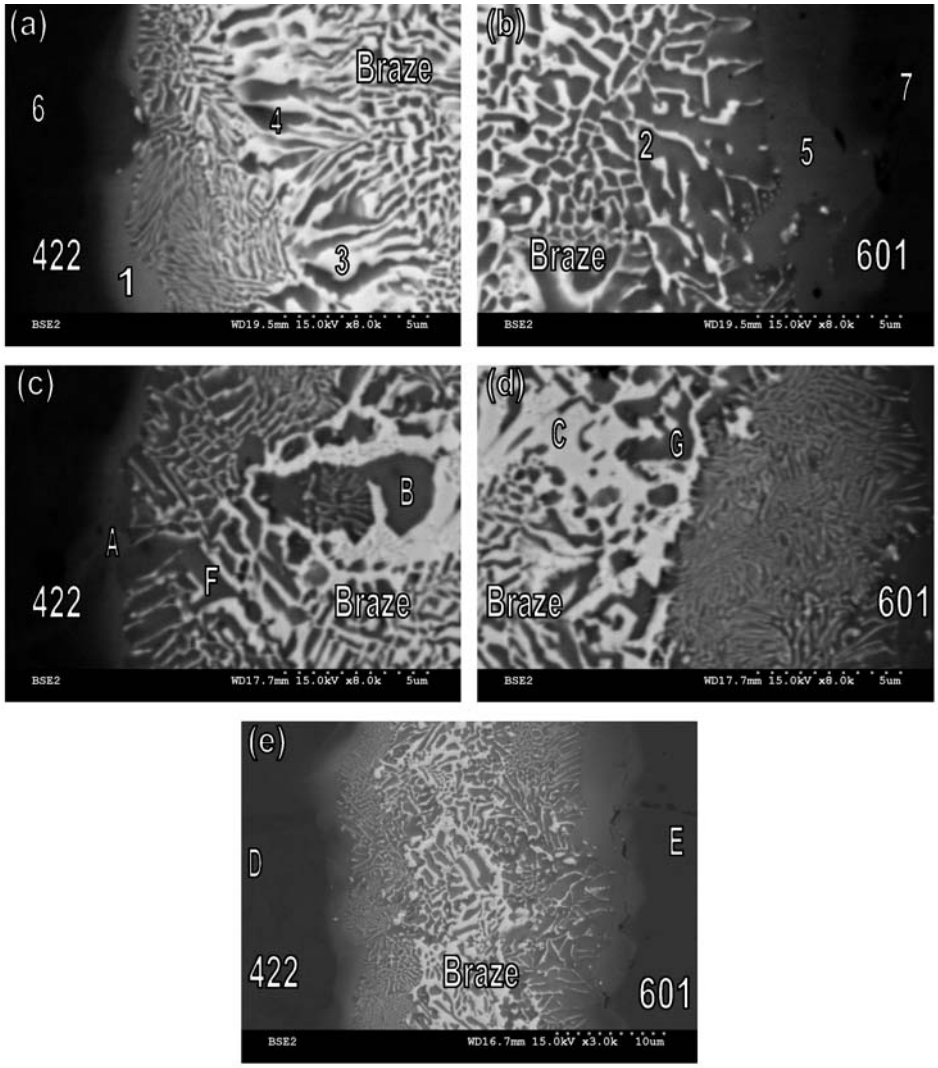

Location (phase)	Au	Pd	Ni	Si	Cr	Mo	V	W	Fe	Mn	Al
1 (Fe,Ni)	6.2	2.1	22.6	2.6	10.0	0.0	0.3	0.4	55.7	0.0	0.3
2 (Ni-rich)	10.8	2.8	57.6	3.4	7.2	0.0	0.1	0.3	17.5	0.0	0.3
3 (Au-rich)	50.8	9.0	16.0	7.1	7.1	0.0	0.5	0.8	8.6	0.2	0.0
4 (Ni-rich)	11.3	3.3	53.9	3.6	6.9	0.0	0.0	0.4	20.3	0.0	0.3
5 (Ni-rich)	3.9	0.8	59.6	1.3	18.8	0.0	0.2	0.0	14.2	0.4	0.9
6 (422SS)	0.0	0.0	1.2	1.5	12.5	0.5	0.3	0.2	82.7	0.9	0.1
7 (IN601)	0.0	0.1	57.6	0.5	24.0	0.0	0.0	0.0	15.2	0.2	2.4
A (Fe,Ni)	3.7	1.3	17.2	2.0	11.7	0.0	0.2	0.5	63.1	0.1	0.2
B (Ni-rich)	11.4	2.8	46.6	3.4	9.3	0.0	0.1	0.6	24.3	0.3	1.2
C (Au-rich)	47.4	8.8	14.9	6.5	7.5	0.0	0.4	1.4	11.3	1.5	0.4
D (422SS)	0.0	0.0	0.7	1.5	13.4	0.6	0.2	0.8	82.0	0.8	0.0
E (IN601)	0.0	0.0	57.8	0.5	24.1	0.0	0.0	0.0	14.8	0.3	2.6
F (Fe,Ni)	6.9	2.5	39.1	2.9	9.6	0.0	0.0	0.6	37.7	0.4	0.4
G (Ni-rich)	13.2	3.4	45.9	3.9	9.4	0.0	0.3	1.2	22.1	0.0	0.7

Figure 6 The SEM BEIs and EDS chemical analysis results of infrared brazed joints at 1100°C for (a)(b) 180 s and (c)–(e) 300 s.

the difference in microstructure between infrared brazed joints for 180 and 300 s brazing time is not significant, the shear test of only infrared brazed specimen for 180 s is performed in the experiment. The infrared brazed joint at 1050°C for 180 s demonstrates the highest average shear strength up to 362 MPa. Additionally, the shear strength of the brazed joint is slightly decreased with increasing the brazing temperature and/or time. It can be attributed to grain size effect of the brazed joint. The strengthening of materials can be performed by grain size reduction, and it is formulized as the Hall-Petch equation [15]. The brazed joint is primarily comprised of Au-rich and Ni-rich phases, and there is no interfacial intermetallic compound observed in the joint. Accordingly, the grain size effect can impose a crucial role in evaluating the shear strength of the joint. For the infrared brazed specimen at 1050°C for 180 s has the finest microstructure, so the highest averaged shear strength is obtained in the test. The microstructure of the brazed joint is coarsened with increasing the brazing temperature and/or time. Accordingly, the average shear strength of the brazed joint is decreased.

Fig. 7 illustrates SEM BEI cross sectional images of the brazed joint after shear test for various brazing

TABLE II Shear strengths of all brazed specimens for various brazing conditions

Brazing type	Temp. (°C)	Time (sec)	Shear strength (MPa)	Average shear strength (MPa)
Infrared	1050	180	364	362
		180	360	
Infrared	1100	180	360	337
		180	314	
Furnace	1050	1200	294	297
		1200	299	

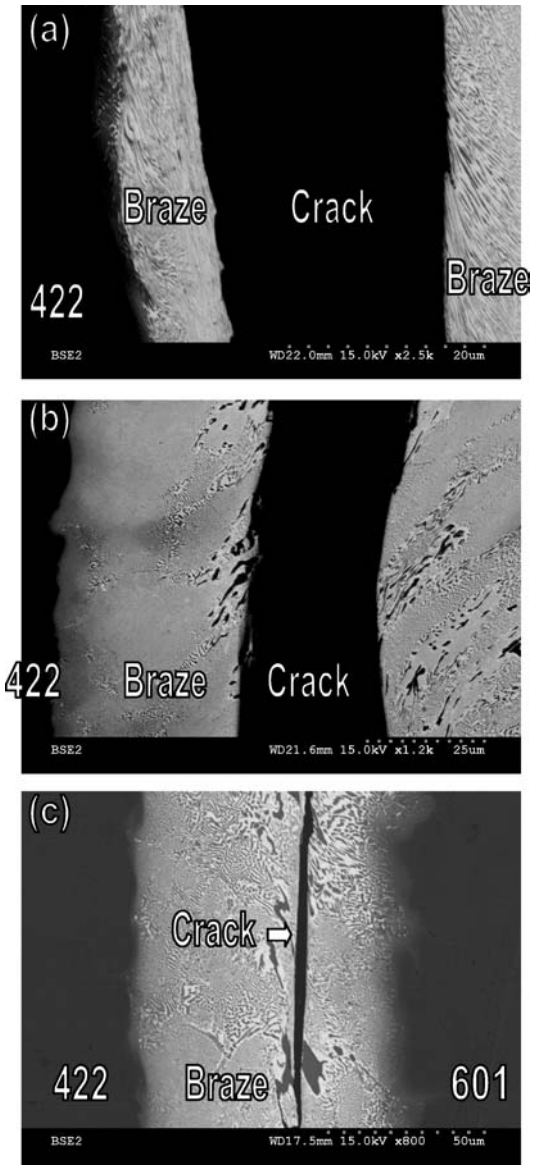

Figure 7 SEM BEI cross sectional images of the brazed joint after shear test: (a) 1050°C ×180 s (infrared brazing), (b) 1100°C ×180 s (infrared brazing) and (c) 1050°C ×1200 s (furnace brazing).

conditions. It is obvious that all brazed specimens are fractured along the braze alloy during the shear test. Significant distortion of the braze alloy is illustrated in Fig. 7. It demonstrates that the braze alloy is ductile and experienced huge amount of plastic deformation before fracture. Fig. 8 shows SEM fractographs of the brazed joint after shear tests. It is very clear that most of the fractured surfaces are dominated by ductile dimples, and it is well consistent with the previous experimental observations.

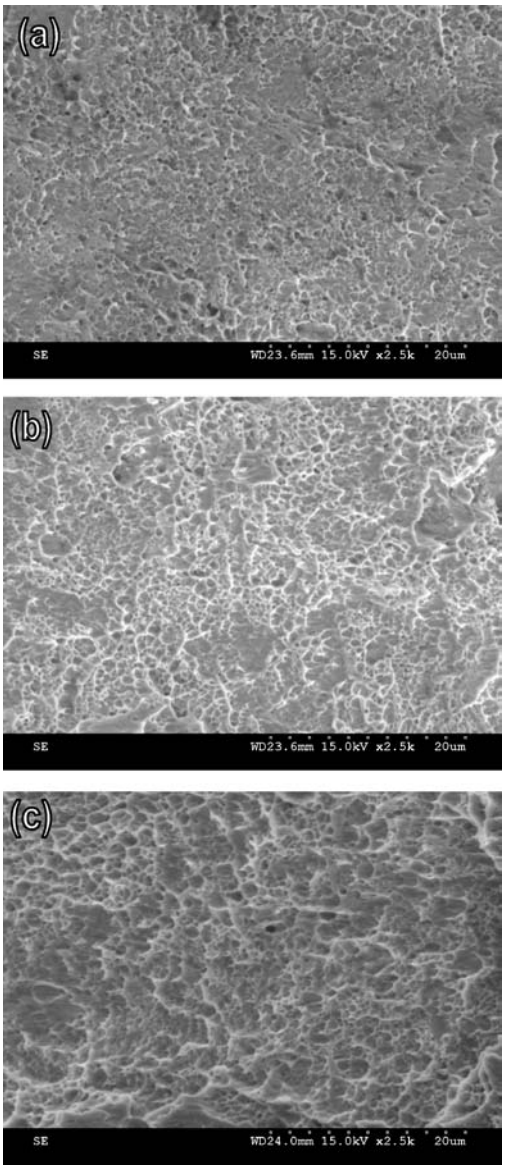

Figure 8 SEM fractographs of the brazed joint after shear test: (a) 1050°C ×180 s (infrared brazing), (b) 1100°C ×180 s (infrared brazing) and (c) 1000°C ×1200 s (furnace brazing).

4. Conclusion

Brazing of Inconel 601 and 422 stainless steel using the 70Au-22Ni-8Pd braze alloy has been evaluated in the experiment. Important conclusions are summarized below.

1. The brazed joint is primarily comprised of Au-rich and Ni-rich phases, and there is no interfacial intermetallic compound observed in the joint. The (Ni,Fe)-rich phase is observed at the interface between 422SS and the braze alloy, and the Ni-rich phase is found at the interface between the braze alloy and IN601. With increasing the brazing temperature and/or time, both microstructures of the brazed joints and interfacial phases are coarsened.

2. The infrared brazed joint at 1050°C for 180 s shows the highest average shear strength of 362 MPa. In contrast, the shear strength of the infrared brazed joint is higher than that of the furnace brazed specimen due to coarsening of the microstructure in the furnace brazed joint.

3. All brazed specimens are fractured along the braze alloy during the shear test. Significant distortion of the braze alloy are found in the experiment. Additionally, dimple dominated fractured surfaces are widely observed in SEM observations due to the presence of ductile Au-rich and Ni-rich phases in the brazed joint.

Acknowledgements

The authors gratefully acknowledge the financial support of this research by the National Science Council (NSC), Republic of China under NSC grant 93-2216-E-002-028.

References

1. W. F. SMITH, in "Structure and Properties of Engineering Alloys" (McGraw-Hill, New York, 1993).
2. J. R. DAVIS, in "Metals Handbook" (ASM International, Materials Park, 1990) Vol. 2.
3. M. SCHWARTZ, in "Brazing" (ASM International, Materials Park, 1987) p. 77.
4. D. L. OLSON, T. A. SIEWERT, S. LIU and G. R. EDWARDS, in "ASM HandbookWelding, Brazing and Soldering" (ASM International, Materials Park, 1993) Vol. 6.
5. G. HUMPSTON and D. M. JACOBSON, in "Principles of Soldering and Brazing" (ASM International, Materials Park, 1993).
6. M. SCHWARTZ, in "Brazing: for the Engineering Technologist" (ASM International, Materials Park, 1993).
7. R. K. SHIUE, S. K. WU and S. Y. CHEN, *Acta Mater.* **51** (2003) 1991.
8. R. K. SHIUE, S. K. WU and C. M. HUNG, *Metall. Mater. Trans.* **33A** (2002) 1765.
9. H. Y. CHAN and R. K. SHIUE, *J. Mater. Sci. Lett.* **22** (2003) 1659.
10. H. Y. CHAN, D. W. LIAW and R. K. SHIUE, *Mater. Lett.* **58** (2004) 1141.
11. R. K. SHIUE, S. K. WU and C. H. CHAN, *J. Alloy Comp.* **372** (2004) 148.
12. H. Y. CHAN, D. W. LIAW and R. K. SHIUE, *Int. J. Refract. Met. Hard Mater*. **22** (2004) 27.
13. P. VILLARS, A. PRINCE and H. OKAMOTO, "Handbook of Ternary Alloy Phase Diagrams" (ASM International, Materials Park, 1995).
14. D. W. LIAW and R. K. SHIUE, *Int. J. Refract. Met. Hard Mater*. **23** (2005) 91.
15. W. D. CALLISTER, in "Materials Science and Engineering an Introduction" (John Wiley & Sons, New York, 1997).

Received 29 September 2004
and accepted 7 February 2005